Parametric Investigation of the Steady-State Response of a Mechanical Seal With Two Flexibly Mounted Rotors

J. Wileman
Georgia Tech Lorraine,
Technopôle Metz 2000,
2-3, rue Marconi,
57070 Metz,
France

I. Green
The George W. Woodruff School of
Mechanical Engineering,
Georgia Institute of Technology,
Atlanta, GA 30332

A parametric analysis is performed to investigate the steady-state dynamic response of a mechanical seal with two flexibly mounted rotors. The effect of changing various inertia, support, and fluid film properties is examined. Short rotors are shown to benefit from gyroscopic aligning moments and to exhibit their maximum steady-state misalignment when one of the shaft speeds is zero. Long rotors experience misaligning gyroscopic moments, but if only one of the two rotors is long then aligning moments from the short rotor can be transmitted through the fluid and counteract the detrimental gyroscopic effect in the long rotor. In this case rotors which corotate are shown to have a higher steady-state misalignment than those which counterrotate because of the reduction of the hydrodynamic moments, thus leading to increased leakage and a higher probability of face contact.

Introduction

Face seal dynamics has been an active area of research for almost three decades. Extensive literature reviews have been provided by Allaire (1984), Tournerie and Frêne (1985), and Etsion (1982, 1985, and 1991). Etsion and Burton (1979) tested a face seal model consisting of a rigidly mounted rotor and a flexibly mounted stator (FMS) subject to initial stator misalignment. They observed self-excited oscillations in the form of precession and nutation of the stator. Lee and Green (1994) experimentally observed higher harmonic oscillations caused by face contact in a flexibly mounted rotor (FMR) seal. Lee and Green (1995a, 1995b) experimentally validated theoretical predictions (Green, 1989) of the dynamic response in an FMR seal.

When a face seal is used to seal between two rotating shafts (Miner, 1992), then the seal will of necessity contain two rotors (Fig. 1). Dynamic analyses of seals with a single rotor and a stator (Green, 1989 and 1990; and Green and Etsion, 1985) have shown that seals in which the rotor is flexibly mounted have a performance advantage over those with a flexibly mounted stator because of the gyroscopic moments which tend to counteract misalignments in the former. This result provokes interest in whether a similar performance improvement can be obtained by flexibly mounting both of the rotors in a two rotor seal. Wileman and Green (1991) described this two flexibly mounted rotor configuration, which is referred to using the abbreviation FMRR, and they defined a kinematic model which was used to derive linearized rotor dynamic coefficients for the incompressible fluid film. Wileman and Green (1997) obtained the equations of motion for the system and presented a method for determining the steady-state response of the system if its geometry and dynamic properties are known. Wileman and Green (1998) performed a stability analysis and established stability criteria for the FMRR configuration. All three of these analyses include the hydrostatic and hydrodynamic effects which result from tilt and coning in the seal, including cross-coupled stiffness effects.

Contributed by the Tribology Division of THE AMERICAN SOCIETY OF MECHANICAL ENGINEERS and presented at the Joint ASME/STLE Tribology Conference, Toronto, Canada, October 25–29, 1998. Manuscript received by the Tribology Division May 7, 1997; revised manuscript received March 2, 1998. Paper No. 98-Trib-5. Associate Technical Editor: J. Frene.

The method devised by Wileman and Green (1997) provides a direct procedure for obtaining the magnitude of the face deflections and misalignments in a completed seal design. Numerical values for the dimensions and support properties of the seal are substituted into a matrix equation which can be solved for the misalignments of both rotors. For reference, these equations are provided in the appendix.

The complexity of the equations which result from expanding this solution symbolically (i.e., without first substituting numerical values) makes it difficult to directly draw general conclusions about the dynamic behavior of the seal. The practicality of the solution method depends upon being able to invert the matrices numerically rather than symbolically, thus requiring a design in which values have been defined for all of the parameters.

This paper overcomes that limitation to obtain some general conclusions about the effects of various seal properties upon the steady-state response. Since it is impossible to do this by completely expanding the analytical solution presented in the appendix, each of the variables in a reference seal design is examined, one at a time, to determine its effect upon the steady-state response.

Wileman and Green (1998) performed a similar parametric analysis to examine the stability of the FMRR configuration. That analysis showed that the stability threshold depended strongly upon the ratio, c, of the transverse to the polar moment of inertia. Short rotors benefit from an aligning gyroscopic effect and are stable over a much larger range of shaft speed than long rotors, for which the gyroscopic effect is detrimental. In systems with a long rotor, the range of speeds over which the seal is stable is skewed toward the counterrotating regime. In seals with two short rotors, the opposite is true.

In the parametric analysis of the steady-state response, we shall see that many of the parameters which had either beneficial or detrimental effects upon seal stability exert similar influences upon the steady-state response.

Parametric Study

The values of the design parameters for the reference seal are presented in Table 1. The reference seal design is based upon the example used by Green (1989) for an analysis of the flexibly mounted rotor configuration. Adhering to these values

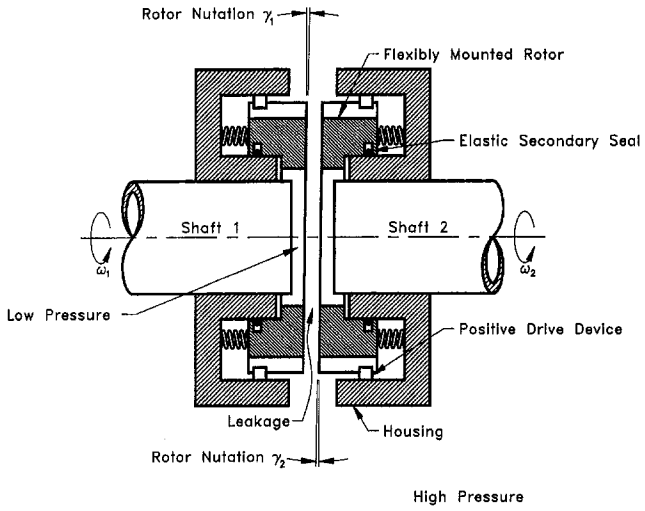

Fig. 1 Schematic of an FMRR mechanical seal

and variations about them will facilitate a comparison between the FMR, FMSR, and FMRR configurations. A negative shaft speed indicates rotation in the sense opposite that indicated by the right-hand rule. For each analysis, the reference values are substituted for all but two of the design parameters, the first of which is different for each analysis while the second is always the speed of shaft 2. The analytical solution (summarized in the appendix) is then expanded to obtain the steady-state misalignment as a function of the undefined variables, and this steady-state misalignment is plotted versus the two independent variables. While it would be desirable to examine the interaction of every variable with every other, the number of variables involved in such an analysis renders it prohibitively complex. Thus the shaft speed, which is the most important influence upon the dynamic response, is always chosen as the second undefined variable.

The parameters tested were the inertia ratios (c_n), moments of inertia (I_n^*), support angular stiffnesses (k_{sn}^*), and support angular damping (d_{sn}^*) of elements 1 and 2; the pressure drop across the sealing dam ($p_o - p_i$); the coning angle (β^*); and the design clearance (C_0). All the values in Table 1 are dimensional, and asterisks are used when necessary to differentiate between a dimensional parameter and a normalized form of the same parameter. The seal design presented in Table 1 is as symmetric as possible so that the effects of asymmetry in the system do not obscure the effects of the changes in the parameter values. Note that the initial support misalignments, γ_{1i}^* and γ_{2i}^*, are assigned values of one radian. Although this is many orders of magnitude larger than any tilt which could occur in a real seal, the unit input makes it possible to compute the transmissibility of the system. Because the equations of motion are linear (Wileman and Green, 1997), this value can be scaled down to the magnitude of the actual tilts without loss of accuracy. All of the misalignment values reported in this work are transmissibilities computed in this way; they are in fact ratios between the output misalignments and the initial misalignments which serve as forcing functions.

Table 1 Parameter values for reference seal design

Variable	Value	Variable	Value
I_1^*	8.0×10^{-4} kg m^2	ω_1^*	−2000 rad/s
I_2^*	8.0×10^{-4} kg m^2	ω_2^*	variable
k_{s1}^*	400 N m	c_1	0.5–3.0
k_{s2}^*	400 N m	c_2	0.5–3.0
d_{s1}^*	0.24 N m s	γ_{1i}^*	1.0 rad
d_{s2}^*	0.24 N m s	γ_{2i}^*	1.0 rad
$p_o - p_i$	10^6 Pa	r_o	0.04 m
β^*	3.125×10^{-3} rad	r_i	0.032 m
C_0	10^{-5} m	μ	5×10^{-4} Pa s

In the FMR analysis, Green (1989) showed that the behavior of the system changed dramatically as a function of the inertia ratio of the rotor, $c_n = I_n^*/J_n^*$. If the value of c approaches 0.5, meaning that the rotor is a short disk, then the gyroscopic moments in the system tend to align the rotor axis with the axis of rotation. If c is large, indicating a rotor which is long relative to its diameter, then the gyroscopic moments tend to make the rotor axis perpendicular to the axis of rotation. It is reasonable to expect that the FMRR seal will be equally sensitive to the value of c, and that the effects of changing the other parameters will be different at the two extremes of c. We shall begin by directly examining the change in the steady-state response with c. Then, when testing the other parameters, the value of c_1 will be maintained at 0.5, but the effect of each parameter will be tested both for $c_2 = 0.5$ (a short rotor) and for $c_2 = 3$ (a long rotor). We shall see that the results confirm the importance of the inertia ratio upon the effects of changing the other parameters.

Nomenclature

c_n = inertia ratio of element n, I_n/J_n
C_0 = equilibrium centerline clearance
d_{11} = fluid film damping coefficient (normalized), $2\pi R_m^3 G_0$
d_{sn}^* = support damping coefficient, angular mode, element n
d = normalized damping coefficient, $d^*\omega_{\text{ref}} C_0/Sr_o^4$
E_0 = stiffness parameter, $(1 - R_i)R_m/[2 + \beta(1 - R_i)]$
G_0 = damping parameter, $\{\ln[1 + \beta(1 - R_i)] - 2\beta(1 - R_i)/[2 + \beta(1 - R_i)]\}/\beta^3(1 - R_i)^2$
I_n^* = transverse moment of inertia (element n)
I_n = normalized transverse moment of inertia, $I^*\omega_{\text{ref}}^2 C_0/Sr_o^4$
J_n^* = polar moment of inertia (element n)
J_n = normalized polar moment of inertia, $J^*\omega_{\text{ref}}^2 C_0/Sr_o^4$
k_{11} = fluid film stiffness coefficient (normalized), $\pi(P_o - P_i)(\beta R_i - 1)E_0^2$
k_{sn}^* = support stiffness coefficient, angular mode, element n
k = normalized stiffness coefficient, k^*C_0/Sr_o^4
p = pressure
P = normalized pressure, p/S
r = radius
R = normalized radius, r/r_o
S = seal parameter, $6\mu\omega_{\text{ref}}(r_o/C_0)^2(1 - R_i)^2$
t^* = time
t = normalized time, $\omega_2 t^*$
β^* = coning angle (radians)
β = normalized coning angle, $\beta^* r_o/C_0$
γ^* = relative tilt angle (radians)
γ_n^* = tilt angle of element n (radians)
γ_{ni}^* = initial misalignment of element n support (radians)
γ = normalized tilt, $\gamma^* r_o/C_0$
μ = viscosity
ω_n^* = shaft angular speed of element n
ω_n = normalized shaft speed, $\omega_n^*/\omega_{\text{ref}}$
ω_{ref} = reference shaft speed (Used for Normalization)

Subscripts

0 = equilibrium value
i = inner radius
n = element number (n = 1 or 2)
o = outer radius

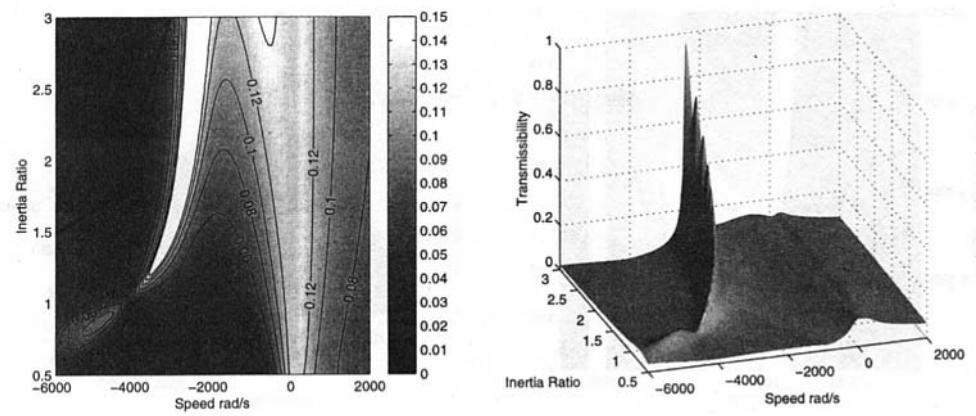

Fig. 2 Maximum relative misalignment versus element 2 shaft speed (rad/s) and inertia ratio I_2/J_2; $c_1 = 0.5$. (Unstable range is upper left portion of contour plot.)

Throughout the analyses, the speed of element 1 (ω_1^*) was maintained at −2000 rad/s. Each of the steady-state analyses presented here consists of simultaneously varying the other shaft speed, ω_2^*, and the value of one of the design parameters mentioned above. The results of the analyses (Figs. 2 to 7) are obtained as plots of the maximum relative misalignment of the two elements versus a range of the parameter being tested and of ω_2^*, which was always varied between −6000 rad/s and 2000 rad/s. Because ω_1^* was negative, a negative value of ω_2^* indicates corotation of the two shafts while a positive value of ω_2^* corresponds to counterrotation. When $\omega_2^* = 0$, the system represents the special case of the FMSR configuration, in which the system contains a stator and a single rotor, each of which is flexibly mounted.

For each parameter, an analysis is performed both for a short and a long rotor, and the plots resulting from all twenty analyses have been presented by Wileman (1994). For conciseness, only the most significant of those plots are included here, but the results of all twenty analyses will be discussed. Each of the figures 2 to 7 presents the data as both a surface plot and a contour plot. The vertical axis of the surface plot is the maximum relative misalignment of the two elements at steady state for the case in which both γ_{1i}^* and γ_{2i}^* are equal to unity. The contour plot is included to facilitate matching the peaks in the curve with corresponding values on the horizontal axes.

It should be realized that the existence of a steady-state solution does not guarantee that the seal will actually reach steady state. The steady-state solution is the particular solution of the equations of motion, and does not consider the homogeneous solution. Thus, a steady-state solution can be obtained regardless of whether the system is stable or unstable. To supplement the steady-state results, a stability analysis using the method of Wileman and Green (1998) was also performed. The bold lines in Figs. 2 to 5 represent the stability thresholds determined by this analysis. In Figs. 6 and 7 the seal is stable over the entire range of the plots.

Before examining the plots to isolate the effects of individual variables, it is interesting to remark the general effect of shaft speed evident in many of the plots. As expected, this effect was dependent upon the inertia ratio of element 2. When both c_1 and c_2 are 0.5, the maximum relative tilt always shows a peak near $\omega_2^* = 0$. When the speed is zero (i.e., the FMSR configuration), the gyroscopic moments which tend to align element 2 disappear, causing an increase in the response. Even at this peak, however, the response was below 0.2 in every case, representing a relatively small transmissibility.

When $c_2 = 3$, corresponding to a long rotor, the gyroscopic moments will tend to misalign the rotor, increasing its relative tilt. In this case, the gyroscopic moments which tend to align the short disk of rotor 1 are transmitted through the fluid film to rotor 2, counteracting the misaligning gyroscopic moments of the long rotor. In the vicinity of exact corotation, when $\omega_2^* \approx \omega_1^*$, the hydrodynamic interaction of the elements is minimum, leading to the peak in the steady-state relative misalignment seen in the plots. The maximum misalignments in this case are nearly an order of magnitude higher than those found when both rotors are short, indicating a far inferior steady-state performance.

Another interesting observation is the proximity of the stability threshold to the peak steady-state response in Figs. 2 to 5.

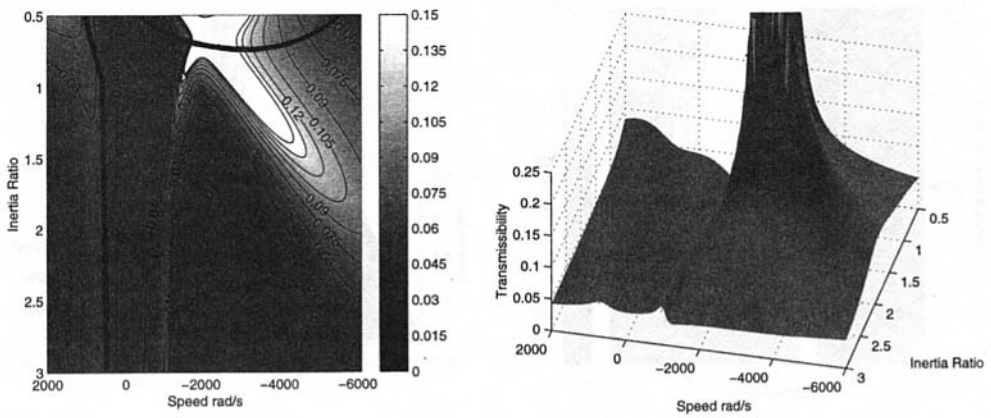

Fig. 3 Maximum relative misalignment versus element 2 shaft speed (rad/s) and inertia ratio I_2/J_2; $c_1 = 3.0$. (Unstable range is lower right portion of contour plot.)

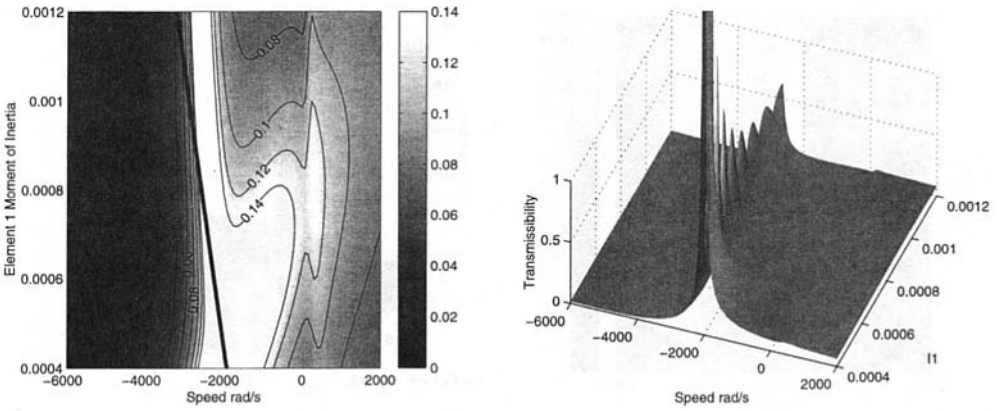

Fig. 4 Maximum relative misalignment versus element 2 shaft speed (rad/s) and element 1 moment of inertia (kg m²); c_2 = 3.0. (Unstable range is left half of contour plot.)

This indicates that both undesirable effects can be avoided with a single seal design.

The Inertia Ratio

In the first two analyses, the inertia ratio of rotor 2, c_2, was varied between 0.5 and 3. Figure 2 shows the result when rotor 1 is short ($c_1 = 0.5$), and Fig. 3 shows the result when $c_1 = 3$.

Figure 2 reveals that when both elements are short, the relative misalignment is minimal because the gyroscopic moments tend to align the elements individually. As the inertia ratio of element 2 begins to increase, the relative misalignment increases because the gyroscopic moments acting upon the two elements have opposite effects. If one of the elements has a low value of c while the other has a high value, then the misalignment of the longer element will tend to be reduced by the hydrodynamic moments, which transfer restoring moments from the short rotor. In Fig. 2 this is apparent as a peak in the relative misalignment near $\omega_1^* = \omega_2^*$, the condition at which the hydrodynamic moments vanish.

In Fig. 3, in which $c_1 = 3$, the relative misalignment shows a peak at $\omega_2^* = \omega_1^*$ and $c_2 = 0.5$. This result is expected, as this condition is simply the reverse of the situation which causes the peak response in Fig. 2. It is interesting to note, however, that when both rotors have high values of c, the response does not increase. This surprising result can be understood by examining the absolute misalignments of the two elements. When both c_1 and c_2 are 3, the absolute misalignments of the two elements are quite large. However, in this example at least, the misalignments are nearly in phase, so that the relative misalignment is small.

The Moments of Inertia

In the remainder of the analyses, the inertia ratio of element 1 was held constant at 0.5. The effect of each of the remaining parameters upon the response was tested when the inertia ratio of element 2 was 0.5 and again when it was 3.0.

For $c_2 = 0.5$, the system is nearly independent of the moments of inertia of both elements. Because both c_1 and c_2 are held fixed, the values of J change in direct proportion to those of I in these analyses. Thus, for the cases in which both elements are short, the two elements align themselves independently because of their gyroscopic moments, and the relative magnitudes of these gyroscopic moments are unimportant.

Figures 4 and 5 show the responses of the system to I_1^* and I_2^*, respectively, when $c_2 = 3$. In Fig. 4, the response shows a peak at $\omega_2^* \approx \omega_1^*$ as the fluid coupling disappears and the unfavorable gyroscopic moment of the long rotor causes the relative misalignment to increase. This behavior is amplified as I_1^* decreases and the relative magnitude of the aligning moment of the short element decreases along with it. Figure 5 also shows a peak in the response when $\omega_1^* \approx \omega_2^*$, but with the response increasing as I_2^* increases. Again this results from an increase in the misaligning moment of the long rotor relative to the aligning moment of the short rotor, with the maximum relative misalignment occurring when the hydrodynamic effect vanishes. It is interesting to note that the peak steady-state re-

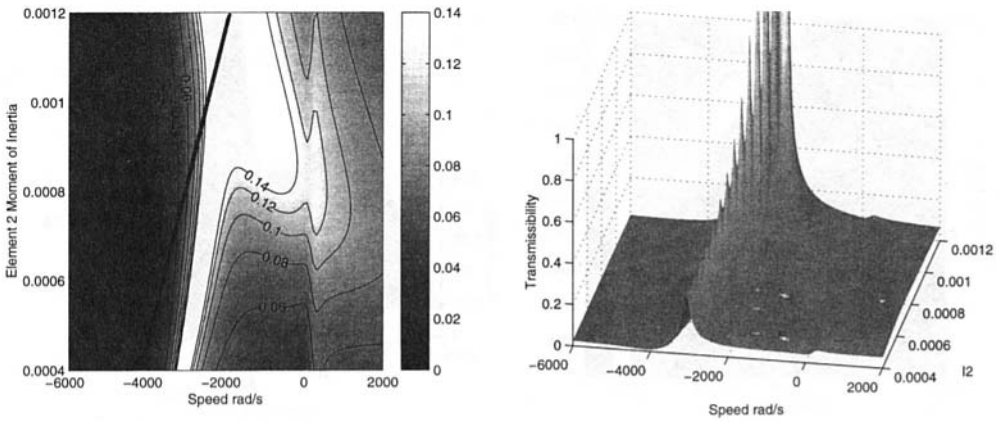

Fig. 5 Maximum relative misalignment versus element 2 shaft speed (rad/s) and element 2 moment of inertia (kg m²); c_2 = 3.0. (Unstable range is left half of contour plot.)

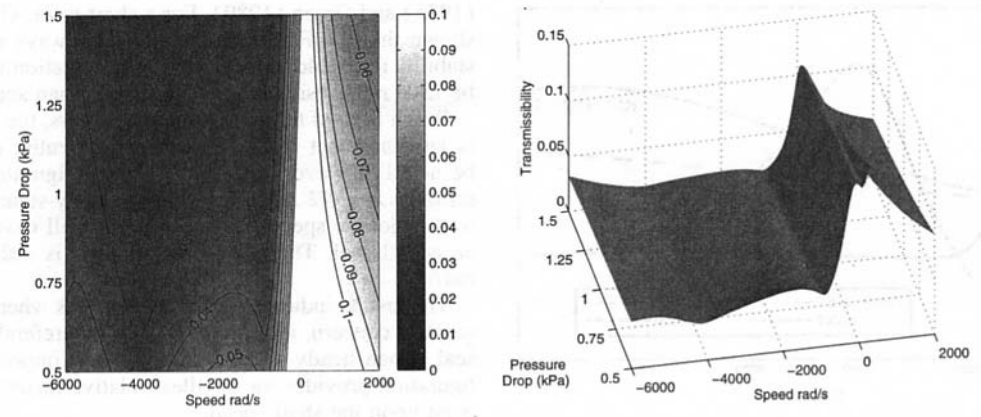

Fig. 6 Maximum relative misalignment versus element 2 shaft speed (rad/s) and pressure drop (Pa); $c_2 = 0.5$

sponse and the stability threshold are very close to one another. Hence, exact corotation is clearly undesirable in this case.

Support Properties

For both short and long rotors the response is nearly independent of the support stiffness of element 1, k_{s1}^*, except for when the speed of element 2 is zero. When $\omega_2^* = 0$, the response shows a slight linear increase with k_{s1}^* for both $c_2 = 0.5$ and $c_2 = 3.0$. The effect of k_{s2}^* is nearly identical to that of k_{s1}^* when rotor 2 is short. Dependence upon the support stiffness is noticeable only when ω_2^* is zero, and even then the change is slight. When $c_2 = 3$, however, the behavior is qualitatively different. In this case the dependence upon k_{s2}^* is evident only when $\omega_2^* = \omega_1^*$, and the response shows a significant peak when $k_{s2}^* = k_{s1}^*$.

The effect of the support damping of element 1 and that of element 2 are nearly identical under all conditions. The response of the system is independent of support damping except at $\omega_2^* = 0$. Here, the response of the system increases slightly as the damping approaches zero. This effect is somewhat more pronounced for the effect of d_{s2}^* when $c_2 = 3$.

The fact that the support properties affect the short rotor only when $\omega_2^* = 0$ indicates that the gyroscopic moment dominates those exerted by the support. When the gyroscopic moment vanishes, the response shows a slight linear increase with support stiffness, as would be expected from the equations of motion in the shaft-fixed system (Wileman and Green, 1997), in which the forcing functions are directly proportional to the support stiffnesses.

Fluid Film Properties

The effects of the pressure drop, coning angle, and design clearance upon the steady-state response are most easily understood by considering their effects upon the fluid film stiffness and damping. The pressure drop across the sealing dam affects only the hydrostatic stiffness of the fluid. Increasing the pressure drop increases the fluid stiffness and should tend to reduce the relative misalignment in every case. This is evident in Fig. 6 at $\omega_2^* = 0$, where there is a slight decrease in the response of the short rotor as the pressure drop increases. When element 2 is not rotating, its own gyroscopic restoring moment vanishes. The increase in the fluid film stiffness caused by an increase in the pressure drop allows more of the restoring moments acting upon element 1 to be transmitted through the fluid film to element 2, thus reducing the relative misalignment.

When $c_2 = 3$, the peak response occurs as usual when the hydrodynamic effect decreases at $\omega_2^* \approx \omega_1^*$. The response increases as the pressure drop decreases. Again, this is expected as decreasing the fluid stiffness decreases the restoring moments which it can transmit to the long element.

The effect of the coning angle is more complex, as both the stiffness and damping of the fluid film depend upon it. The two effects can be separated somewhat by noting that the damping decreases monotonically as the coning angle increases, while the stiffness reaches a maximum value at the optimum coning angle of about 12.5 (normalized) and decreases as the coning deviates from the optimum (Green and Etsion, 1983). It was found that the response of the system increases monotonically with the coning angle (Wileman, 1994); thus, we can conclude

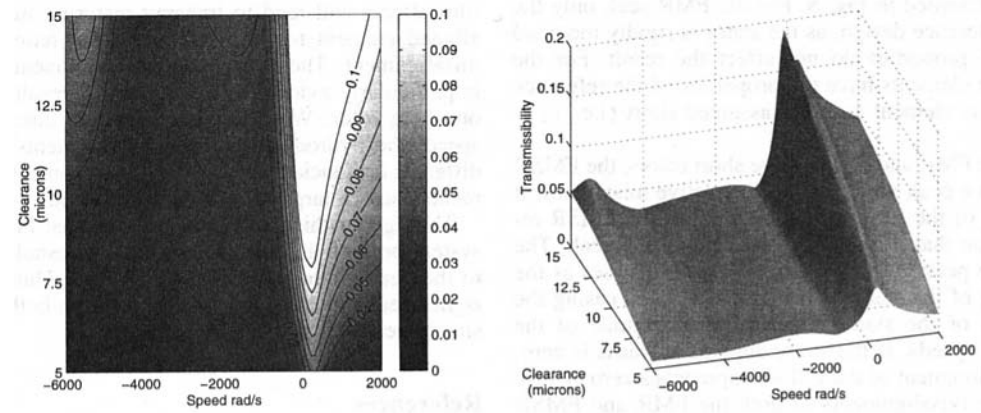

Fig. 7 Maximum relative misalignment versus element 2 shaft speed (rad/s) and design clearance (m); $c_2 = 0.5$

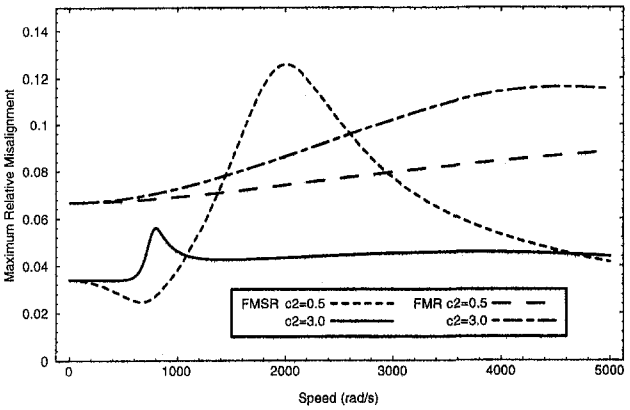

Fig. 8 Comparison of FMR and FMSR configurations

that the change in damping is more significant than that of the stiffness. The effect of the coning angle upon the system is very slight, however, and evident only when ω_2^* is zero. The increase in the misalignment with the coning angle may indicate that the fluid damping, which decreases as the coning angle increases, acts to bring the two elements more closely into alignment.

The design clearance affects the hydrostatic stiffness in a manner opposite that of the pressure drop, so it is not surprising that the system is most sensitive to changes in the clearance at the same speeds as it is most sensitive to the pressure drop. When $c_2 = 0.5$ (Fig. 7), the effect is again noticeable only when $\omega_2^* = 0$, and the response of the system increases here as the clearance increases. The resulting decrease in the fluid film stiffness has the same effect as the stiffness reduction which resulted from decreasing the pressure drop.

The $c_2 = 3$ behavior is also opposite to that for the pressure drop. The fluid stiffness decreases with increasing clearance, causing an increase in the relative misalignment.

Comparison of the FMR and FMSR Configurations

The performance of the FMRR and FMR configurations cannot be compared because an FMR seal cannot be used in applications with two rotors. It is possible to use an FMSR seal in most places that an FMR seal can be used, however. Recall that the FMSR (or Flexibly Mounted Stator and Rotor) configuration consists of two flexibly mounted elements: one which rotates with a shaft and one which is attached to a stationary housing. Thus, the difference between the FMR and FMSR configurations is that the stator is rigidly mounted in the FMR configuration while it is flexibly mounted in the FMSR configuration. The steady-state responses for the FMR and FMSR reference seals are presented in Fig. 8. For the FMR seal, only the rotor uses the reference design, as the stator is rigidly mounted and its dynamic properties do not affect the result. For the FMSR seal, both elements have the properties of the reference case. The stator is element 1 and is assumed short (i.e., $c_1 = 0.5$).

When both the FMR and FMSR have short rotors, the FMSR response exhibits a peak which makes its relative misalignment greater than that of the FMR configuration, but the FMSR response is less than that of the FMR away from this peak. The magnitude of the peak in the FMSR response decreases as the support damping of the stator is increased, and decreasing the support stiffness of the stator reduces the magnitude of the response at high speeds. If the stator support stiffness is zero, the relative misalignment of the FMSR approaches zero at very high speeds. The misalignments of both the FMR and FMSR configurations are much less than those of the flexibly mounted stator (FMS) configuration as presented by Green and Etsion (1985) and Green (1989). For a short rotor, Green (1990) has shown that the FMR configuration is always stable, while the stability threshold for the FMSR configuration was computed to be 7309 rad/s using the criteria of Wileman and Green (1998).

When both of the seals have long rotors, the FMSR response is less than that of the FMR over the entire range. It should be noted, however, that the FMSR configuration will become unstable at 1772 rad/s, so that the steady-state solution shown in the plot for speeds higher than this will never be reached in an actual seal. The FMR configuration is stable up to 12081 rad/s.

The results indicate that in applications where stability is the greatest concern, an FMR seal may be preferable to an FMSR seal. When steady-state response is more important, which configuration provides the smallest relative misalignment will depend upon the shaft speed.

Conclusions

It should be emphasized that the results presented here are based upon a single reference design, and care should be taken in trying to generalize them to other seals. Several trends which appear in the results are nonetheless worthy of note.

When both elements are short, the maximum steady-state response occurs when one of the shaft speeds is zero. When one element is short and one is long, however, a significant and undesirable relative misalignment results when both shafts turn in the same direction at the same speed. These results can be understood by considering the effects of the individual parts of the system. The gyroscopic moments will tend to align either element (reducing the response) when c for that element is less than one, and will tend to misalign the element when c is greater than one. These effects will increase with the absolute angular velocity of the element, and will disappear when the angular velocity is zero. Thus, the maximum misalignment of the short rotor case occurs when one of the velocities is zero.

Increasing the support stiffness and damping makes the misalignment of the rotor more closely match that of the flexible support, and this will tend to increase the effect of the forcing function. The flexible support moments also tend to counteract the effects of the gyroscopic moments. It is reasonable, therefore, to design seals with the smallest possible support stiffness and damping.

The pressure drop, coning, and design clearance affect the fluid film stiffness and damping. Increasing either the stiffness or the damping will tend to increase the coupling between the elements. In cases where the two elements tend to align themselves independently (two short rotors), this coupling is likely to increase the relative misalignment because of the phase and frequency differences between the two forcing functions. In cases where only one of the two elements tends toward misalignment (one short and one long rotor), however, the fluid film effects will tend to transmit restoring moments from the aligned element to the misaligned one, reducing the relative misalignment. The hydrodynamic component of these effects is particularly evident in the numerical results for the case of one long rotor. When the two elements corotate at the same speed, the hydrodynamic restoring moments vanish, and the different tendencies of the gyroscopic moments of the two elements cause a large relative misalignment.

Throughout this study it was found that in cases where the system became unstable, the stability threshold was very close to the peak in the steady-state response. Thus, a properly designed seal should be capable of avoiding both of these effects simultaneously.

References

Allaire, P. E., 1984, "Noncontacting Face Seals for Nuclear Applications—A Literature Review," *Lubrication Engineering*, Vol. 40, No. 6, pp. 344–351.

Etsion, I., 1982, "A Review of Mechanical Face Seal Dynamics," *The Shock and Vibration Digest,* Vol. 14, No. 2, pp. 9–14.

Etsion, I., 1985, "Mechanical Face Seal Dynamics Update," *The Shock and Vibration Digest,* Vol. 17, No. 4, pp. 11–15.

Etsion, I., 1991, "Mechanical Face Seal Dynamics 1985–1989," *The Shock and Vibration Digest,* Vol. 23, No. 4, pp. 3–7.

Etsion, I., and Burton, R. A., 1979, "Observation of Self-Excited Wobble in Face Seals," ASME JOURNAL OF LUBRICATION TECHNOLOGY, Vol. 101, pp. 526–528.

Green, I., and Etsion, I., 1983, "Fluid Film Dynamic Coefficients in Mechanical Face Seals," ASME JOURNAL OF LUBRICATION TECHNOLOGY, Vol. 105, pp. 297–302.

Green, I., and Etsion, I., 1985, "Stability Threshold and Steady-State Response of Noncontacting Coned-Face Seals," *ASLE Transactions,* Vol. 28, No. 4, pp. 449–460.

Green, I., 1989, "Gyroscopic and Support Effects on the Steady-State Response of a Noncontacting Flexibly Mounted Rotor Mechanical Face Seal," ASME JOURNAL OF TRIBOLOGY, Vol. 111, pp. 200–208.

Green, I., 1990, "Gyroscopic and Damping Effects on the Stability of a Noncontacting Flexibly-Mounted Rotor Mechanical Face Seal," *Dynamics of Rotating Machinery,* Hemisphere Publishing, pp. 153–173.

Lee, A. S., and Green, I., 1994, "Higher Harmonic Oscillation in a Flexibly Mounted Rotor Mechanical Seal Test Rig," ASME *Journal of Vibration and Acoustics,* Vol. 116, No. 2, pp. 161–167.

Lee, A. S., and Green, I., 1995a, "Physical Modeling and Data Analysis of the Dynamic Response of a Flexibly Mounted Rotor Mechanical Seal," ASME JOURNAL OF TRIBOLOGY, Vol. 177, No. 1, pp. 130–135.

Lee, A. S., and Green, I., 1995b, "An Experimental Investigation of the Steady-State Response of a Noncontacting Flexibly Mounted Rotor Mechanical Face Seal," ASME JOURNAL OF TRIBOLOGY, Vol. 177, No. 1, pp. 153–159.

Miner, J. R., Mohn, J. H., Grant, D. H., and Lee, V. H., 1992, "High Speed Seal Development, Part I," United Technologies, Pratt and Whitney, Interim Report to Wright Laboratory, Air Force Materiel Command, WL-TR-92-2101.

Tournerie, B., and Frêne, J., 1985, "Les joints d'étanchéité à faces radiales: étude bibliographique," *Matériaux Mécanique Electricité,* No. 410, pp. 44–52.

Wileman, J. M., and Green, I., 1991, "The Rotordynamic Coefficients of Mechanical Seals Having Two Flexibly Mounted Rotors," ASME JOURNAL OF TRIBOLOGY, Vol. 113, No. 4, pp. 795–804.

Wileman, J. M., 1994, "Dynamic Analysis of Eccentric Mechanical Face Seals," Doctoral dissertation, Georgia Institute of Technology.

Wileman, J. M., and Green, I., 1997, "Steady-State Analysis of Mechanical Seals with Two Flexibly Mounted Rotors," ASME JOURNAL OF TRIBOLOGY, Vol. 119, No. 1, Jan., pp. 200–204.

Wileman, J. M., and Green, I., 1998, "Stability Analysis of Mechanical Seals with Two Flexibly Mounted Rotors," ASME JOURNAL OF TRIBOLOGY, Vol. 120, No. 2, pp. 145–151.

APPENDIX

Steady-State Equations of Motion

The steady-state solution to the equations of motion is obtained by resolving them into components in the reference frames which rotate with the two shafts. The forcing functions result from the initial misalignments of the two flexible supports, and each of these forcing functions is constant when expressed in the rotating reference attached to its own shaft (Wileman and Green, 1997). This permits the equations to be reduced to a set of linear algebraic equations which can be solved for the steady-state misalignments.

This process must be performed once for each of the two support misalignments since the two misalignments are constant in different systems. The two solutions are combined to provide the total response amplitude. In the shaft 1 system, the equations are

$$(\mathbf{A_2}) \begin{Bmatrix} \gamma_{2I} \\ \gamma_{2J} \\ \gamma_{1I} \\ \gamma_{1J} \end{Bmatrix} = \begin{Bmatrix} k_{s2}\gamma_{2i} \\ 0 \\ 0 \\ 0 \end{Bmatrix} \tag{1}$$

where

$$\mathbf{A_2} = \begin{pmatrix} (J_2 - I_2)\omega_2^2 + k_{11} + k_{s2} & -\frac{1}{2}d_{11}(\omega_2 - \omega_1) & -k_{11} & \frac{1}{2}d_{11}(\omega_2 - \omega_1) \\ \frac{1}{2}d_{11}(\omega_2 - \omega_1) & (J_2 - I_2)\omega_2^2 + k_{11} + k_{s2} & -\frac{1}{2}d_{11}(\omega_2 - \omega_1) & -k_{11} \\ -k_{11} & \frac{1}{2}d_{11}(\omega_2 - \omega_1) & (J_1\omega_1 - I_1\omega_2)\omega_2 + k_{11} + k_{s1} & \left(d_{s1} - \frac{d_{11}}{2}\right)(\omega_2 - \omega_1) \\ -\frac{1}{2}d_{11}(\omega_2 - \omega_1) & -k_{11} & -\left(d_{s1} - \frac{d_{11}}{2}\right)(\omega_2 - \omega_1) & (J_1\omega_1 - I_1\omega_2)\omega_2 + k_{11} + k_{s1} \end{pmatrix}$$

The shaft speeds are normalized using a reference speed, ω_{ref}, which will usually be the absolute value of the higher shaft speed.

In the shaft 2 system the equations are

$$(\mathbf{A_1}) \begin{Bmatrix} \gamma_{2I} \\ \gamma_{2J} \\ \gamma_{1I} \\ \gamma_{1J} \end{Bmatrix} = \begin{Bmatrix} 0 \\ 0 \\ k_{s1}\gamma_{1i} \\ 0 \end{Bmatrix} \tag{2}$$

where

$$\mathbf{A_1} = \begin{pmatrix} (J_2\omega_2 - I_2\omega_1)\omega_1 + k_{11} + k_{s2} & \left(d_{s2} + \frac{d_{11}}{2}\right)(\omega_2 - \omega_1) & -k_{11} & -\frac{1}{2}d_{11}(\omega_2 - \omega_1) \\ -\left(d_{s2} + \frac{d_{11}}{2}\right)(\omega_2 - \omega_1) & (J_2\omega_2 - I_2\omega_1)\omega_1 + k_{11} + k_{s2} & +\frac{1}{2}d_{11}(\omega_2 - \omega_1) & -k_{11} \\ -k_{11} & -\frac{1}{2}d_{11}(\omega_2 - \omega_1) & (J_1 - I_1)\omega_1^2 + k_{11} + k_{s1} & \frac{1}{2}d_{11}(\omega_2 - \omega_1) \\ \frac{1}{2}d_{11}(\omega_2 - \omega_1) & -k_{11} & -\frac{1}{2}d_{11}(\omega_2 - \omega_1) & (J_1 - I_1)\omega_1^2 + k_{11} + k_{s1} \end{pmatrix}$$

The tilt variables γ_{2I}, γ_{2J}, γ_{1I}, and γ_{1J} represent components of the element tilts (the arabic numeral denotes the element number)

resolved onto the I and J axis. These axes are attached to a coordinate system which rotates with the angular velocity of the support misalignment which acts as the forcing function in the system.

The solution to each of these equations provides the components of the rotating response to a single initial misalignment, γ_{nI} and γ_{nJ}, expressed in the shaft-fixed system. Each of the two solutions represents a constant tilt which precesses at the speed of the associated shaft.

The maximum relative misalignment between the two elements is a more important measure of the seal performance and determines the leakage rate of the seal and whether the two seal faces come into contact. The relative misalignment will consist of contributions from each of the two forcing functions.

To compute the contribution of shaft n, subtract the I and J components of element 1 from those of element 2. This yields the components of the relative misalignment in the shaft-fixed system and preserves the necessary phase information. The magnitude of the relative misalignment is thus

$$\gamma = \sqrt{(\gamma_{2J} - \gamma_{1J})^2 + (\gamma_{2I} - \gamma_{1I})^2}$$

This computation is performed separately for the solution to each of the two forcing functions. The maximum relative misalignment in the actual seal will be the sum of the maximum relative misalignment which results from each of the two forcing functions. Thus, summing the magnitudes of the individual contributions yields the values which will describe the behavior of the seal, and which are plotted in the figures.